Smart Materials and Structures

PAPER • **OPEN ACCESS**

Curing process monitoring of polymeric composites with Gramian angular field and transfer learning-boosted convolutional neural networks

To cite this article: Jianjian Zhu *et al* 2023 *Smart Mater. Struct.* **32** 115017

OPEN ACCESS
IOP Publishing
Smart Materials and Structures
Smart Mater. Struct. **32** (2023) 115017 (11pp)
https://doi.org/10.1088/1361-665X/acfcf8

Curing process monitoring of polymeric composites with Gramian angular field and transfer learning-boosted convolutional neural networks

Jianjian Zhu[1,2,*], **Zhongqing Su**[1,2], **Qingqing Wang**[1,3], **Yinghong Yu**[4], **Jinshan Wen**[4] **and Zhibin Han**[5]

[1] Department of Mechanical Engineering, The Hong Kong Polytechnic University, Kowloon, Hong Kong Special Administrative Region of China, People's Republic of China
[2] The Hong Kong Polytechnic University Shenzhen Research Institute, Shenzhen 518057, People's Republic of China
[3] School of System Design and Intelligent Manufacturing, Southern University of Science and Technology, Shenzhen 518055, People's Republic of China
[4] School of Aerospace Engineering, Xiamen University, Xiamen 361102, People's Republic of China
[5] Department of Mechanical and Automation Engineering, The Chinese University of Hong Kong, Hong Kong Special Administrative Region of China, People's Republic of China

E-mail: zhujj.work@outlook.com

Received 6 May 2023, revised 4 September 2023
Accepted for publication 25 September 2023
Published 6 October 2023

Abstract

Continuous and accurate monitoring of the degree of curing (DoC) is essential for ensuring the structural integrity of fabricated composites during service. Although machine learning (ML) has shown effectiveness in DoC monitoring, its generalization and extendibility are limited when applied to other curing-related scenarios not included in the previous learning process. To break through this bottleneck, we propose a novel DoC monitoring approach that utilizes transfer learning (TL)-boosted convolutional neural networks alongside Gramian angular field-based imaging processing. The effectiveness of the proposed approach is validated through experiments on metal/polymeric composite co-bonded structures and carbon fiber reinforced polymers using raw sensor data separately collected through the electromechanical impedance and fiber Bragg grating (FBG) measurements. Four indicators, accuracy, precision, recall, and F1-score are introduced to evaluate the performance of generalization and extendibility of the proposed approach. The indicator scores of the proposed approach exceed 0.9900 and outperform other conventional ML algorithms on the FBG dataset of the target domain, demonstrating the effectiveness of the proposed approach in reusing the pre-trained base model on the composite curing monitoring issues.

---

[*] Author to whom any correspondence should be addressed.

1361-665X/23/115017+11$33.00 Printed in the UK

Keywords: curing monitoring, polymeric composite, machine learning, transfer learning, convolutional neural networks

(Some figures may appear in colour only in the online journal)

Nomenclatures

Variables	Meanings
C	Capacitance of the piezoelectric wafer
$\bar{\varepsilon}_{33}^{T}$	Dielectric constant of the piezoelectric wafer
a	Radius of the circular piezoelectric wafer
h	Thickness of the circular piezoelectric wafer
d_{31}	Piezoelectric constant
s_{11}^{E}	Compliance coefficient
ν	Poisson's ratio
k_p	Electromechanical coupling coefficient
$Z_{P,\mathrm{sc}}$	Impedance of piezoelectric wafers under short-circuit
Z_{str}	Mechanical impedance of the monitored structure
$J_1(\cdot)$	Bassel function of the first kind and 1-order
$J_0(\cdot)$	Bassel function of the first kind and 0-order
ω	Angular frequency
c_p	Phrase velocity
D	Domains of transfer learning
χ	Feature space
γ	Label space
$P(X)$	Marginal probability
$f(\cdot)$	Objective function of transfer learning
D_S	Source domain
D_T	Target domain
T_S	Tasks of source domain (source tasks)
T_T	Tasks of target domain (target tasks)
I	Unit row vector
$\tilde{T}$	Set of rescaled series data
θ	Arc cosine value of rescaled series data
λ	Wavelength shift
n_0	Effective refractive index of the grating region
Λ	Grating period
$\Delta\lambda_T$	Wavelength shift under the temperature
$\Delta\lambda_\varepsilon$	Wavelength shift under the strain
ΔT	Temperature variation
$\Delta\varepsilon$	Strain variation

1. Introduction

The 'cradle-to-grave'-inspired life cycle assessment and health management of composite structures have been the subject of intensive research over the years. It articulates the continuous monitoring of structural integrity and health status of the composites using onboard sensors in a timely or, preferably, a near real-time manner from curing through service to the end-of-life of the composites, so as to enhance the structural durability, lower the maintenance cost, and extend the residual service life as progressive aging. Particularly, the degree of curing (DoC) is an essential quality-assurance indicator in the 'cradle' stage of polymer-matrix composites and is vital to warrant the structural integrity and performance of the fabricated composites in service.

Due to the features of cost-effectiveness, simplicity of post-signal processing, and high sensitivity to DoC variation, electromechanical impedance (EMI) has proven its advantage over diverse techniques available for DoC monitoring, such as infrared thermal imaging and optoelectronic measurement [1–4]. The EMI method has further been advanced with the increased introduction of machine learning (ML) algorithms [5–9]. Demonstrated application paradigms include the prediction of DoC using simulation data-based ML [10], which concentrates on optimizing the autoclave co-curing process for sandwich composite structures using a decision tree (DT) and random forest [11]. The DoC prediction of the thermosetting prepreg in the compression molding process using an integrated method embracing genetic algorithm and back propagation is explored, and the feasibility is discussed [12]. Though showing effectiveness and promising prospect, conventional ML-driven DoC monitoring is often restricted by the intrinsic bottleneck of ML algorithms, including particularly the poor generalization and inferior extendibility, when ML algorithms are attempted to new scenarios that are not included in the training processing (e.g., different kinds of polymers, different layouts of composites, different types of sensors, etc.) [13–20]. Motivated by this, we develop a new DoC monitoring approach, which comprises the transfer learning (TL)-boosted convolutional neural networks (CNNs), in conjunction with a Gramian angular field (GAF)-based imaging processing.

The proposed approach aims to tackle the bottleneck of applying a pre-trained base model (PBM) to the curing monitoring of composite structures with different layouts. To validate the feasibility and effectiveness of the proposed approach on enhancing generalization capacity and extendibility without the need to increase the training dataset scale, experiments are carried out on polymetric composites with embedded fiber Bragg gratings (FBG) sensors, essentially different from the previous experiments for PBM. Four indicators, accuracy, precision, recall, and F1-score are adopted to assess the performance of the proposed approach. The final results of the proposed approach are discussed and compared with conventional ML algorithms, demonstrating the effectiveness of the proposed approach.

2. Methodology and fundamental

2.1. TL strategy

According to [21, 22], the TL is a multi-task learning framework that tries to learn various tasks simultaneously, even in different scenarios. Therefore, the TL can be utilized to bridge the gap of applying the pre-trained deep learning (DL) models in the source domain to the target domain, as shown in figure 1.

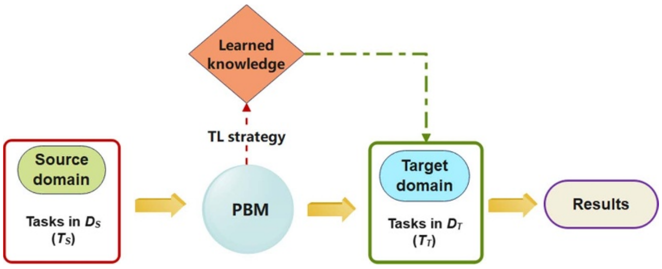

Figure 1. Schematic diagram of transfer learning.

The conventional DL methods are traditionally leveraged for isolated learning tasks, requiring customization every time for a new dataset in other application scenarios, which lack the flexibility to adapt to changes in time-dependent applications. Nevertheless, those limitations can be primarily surmounted by TL, which could implement the knowledge transferring from the source domain to a new target domain.

The TL strategy adopted in this study is taking the PBM as a feature extractor in the reconstructed model. The weight values inside PBM are objective to be reused in a new scenario. The mathematical definition of TL goes as follows: supposing that there is a domain D, which could be described with a two-element tuple, including feature space χ and marginal probability $P(X)$, where X is a set of sample data, defined as $X=\{x_1,x_2,\ldots,x_n\}$ with vectorized element $x_i\,(i=1,2,\ldots,n)$. Then equation (1) can be yielded as:

$$D=\{\chi,P(X)\},X\in\chi. \tag{1}$$

Moreover, suppose there is a task T, which can also be defined as a two-element tuple of the label space γ and an objective function f. The f is described as $P(\gamma|X)$ from the probabilistic perspective. Then the mathematical definition of a task is rendered by equation (2):

$$T=\{\gamma,f\}=\{\gamma,P(\gamma|X)\}. \tag{2}$$

The above-mentioned domain can be further separated into the source domain D_S and the target domain D_T in detail. Accordingly, the tasks can be categorized into the source task T_S and the target task T_T. Considering the framework introduced by equation (1), the TL can be described as applying the knowledge learned from the T_S to solving the T_T. Hence, the defined purpose of this study can be expressed by equation (3):

$$\begin{cases} D_S\neq D_T \\ T_S\neq T_T \end{cases}. \tag{3}$$

According to [23–25], the CNN model is readily available for image-relevant tasks based on various processing layers, such as the convolutional layers, pooling layers, dense layers, etc. The TL strategy boosted by the feature extraction can then be diagrammatically presented in figure 2.

Figure 2 indicates that the reconstructed model contains weight values learned from GAF images of the source domain, which plays the role of 'brain' in a rebuilt model. Three convolution-pooling blocks are frozen to prevent the current weight values from being updated when reused in a new case. The output of Block#3 is bottleneck features that are then vectorized into a column as an input of the classifier followed. The final results of DoC monitoring are exported from the output layer.

2.2. Series data to GAF images

To meet the requirement of TL-boosted CNN, it is necessary to convert sensor data into images. Thus, the method of GAF is introduced to convert all the sensor data obtained at the cradle stage to images. The GAF is an approach that converts series data into visual representations. It involves constructing a matrix from the data, normalizing its rows, computing the Gram matrix through dot products, and converting it into an image using color mapping. The resulting image visually elucidates cyclic patterns and relationships within the original time-series data.

In detail, GAF includes two kinds of image-transformation methods, which are Gramian summation angular field (GASF) and Gramian angular difference field (GADF) [26], given by equations (4) and (5):

$$\mathrm{GASF}=[\cos(\theta_i+\theta_j)]=\tilde{T}'\cdot\tilde{T}-\sqrt{I-\tilde{T}^2}'\cdot\sqrt{I-\tilde{T}^2} \tag{4}$$

$$\mathrm{GADF}=[\sin(\theta_i-\theta_j)]=\sqrt{I-\tilde{T}^2}'\cdot\tilde{T}-\tilde{T}'\cdot\sqrt{I-\tilde{T}^2} \tag{5}$$

where the I denotes the unit row vector; $\tilde{T}$ is the set of rescaled series data; θ is the value of arc cosine based on the data. Specifically, for the data obtained by the EMI and FBG measurement, θ_i can be calculated using the equations (6) and (7). For measured EMI signals, the θ_i can be explained using the equation (6):

$$\theta_i=\arccos\left(\frac{(R_i-\max(R))+(R_i-\min(R))}{\max(R)-\min(R)}\right),\quad i=1,2,3,\ldots,n \tag{6}$$

where $R=\{R_1,R_2,\ldots,R_i,\ldots,R_n\}$. R_i is the real part of the EMI signals, which are actual resistance values, that are measured by piezoelectric sensors. Similarly, for measured FBG signals, the θ_i can be explained using the equation (7):

$$\theta_i=\arccos\left(\frac{(\varepsilon_i-\max(\varepsilon))+(\varepsilon_i-\min(\varepsilon))}{\max(\varepsilon)-\min(\varepsilon)}\right),\quad i=1,2,3,\ldots,n \tag{7}$$

where $\varepsilon=\{\varepsilon_1,\varepsilon_2,\ldots,\varepsilon_i,\ldots,\varepsilon_n\}$. ε_i is micro-strain values that are measured by optical sensors.

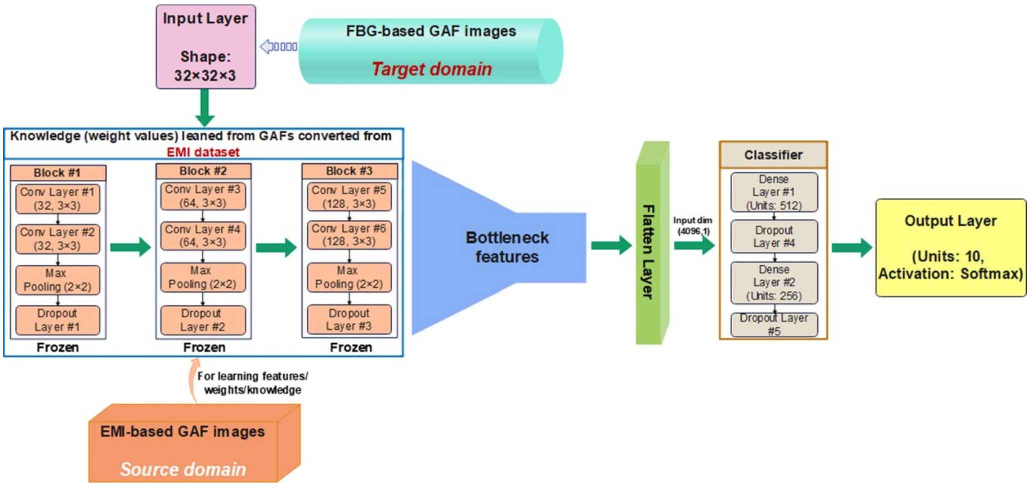

Figure 2. Architecture of rebuilt CNN model boosted by TL strategy.

By referring to the well-known Gramian matrix, equations (4) and (5) can be further deduced as equations (8) and (9), which are the core equations implementing the process of sensor data to images

$$\mathrm{GASF}=\begin{bmatrix}\cos\left(\theta_1+\theta_1\right) & \cos\left(\theta_1+\theta_2\right) & \cdots & \cos\left(\theta_1+\theta_n\right)\\ \cos\left(\theta_2+\theta_1\right) & \cos\left(\theta_2+\theta_2\right) & \cdots & \cos\left(\theta_2+\theta_n\right)\\ \vdots & \vdots & \ddots & \vdots\\ \cos\left(\theta_n+\theta_1\right) & \cos\left(\theta_n+\theta_2\right) & \cdots & \cos\left(\theta_n+\theta_n\right)\end{bmatrix} \tag{8}$$

$$\mathrm{GADF}=\begin{bmatrix}\sin\left(\theta_1-\theta_1\right) & \sin\left(\theta_1-\theta_2\right) & \cdots & \sin\left(\theta_1-\theta_n\right)\\ \sin\left(\theta_2-\theta_1\right) & \sin\left(\theta_2-\theta_2\right) & \cdots & \sin\left(\theta_2-\theta_n\right)\\ \vdots & \vdots & \ddots & \vdots\\ \sin\left(\theta_n-\theta_1\right) & \sin\left(\theta_n-\theta_2\right) & \cdots & \sin\left(\theta_n-\theta_n\right)\end{bmatrix}. \tag{9}$$

2.3. Fundamental of EMI and FBG measurements

The piezoelectric wafer and host structure are usually connected by adhesive. The principle of EMI based on a piezoelectric wafer is that when an electrical signal is applied to the piezoelectric material, it produces mechanical deformation, which in turn causes a voltage change in the transducer. This voltage can then be converted into impedance or admittance signals to measure the mechanical performance deterioration indirectly. Moreover, the piezoelectric wafer simultaneously serves as the actuator and receiver in the EMI measurement. The equation for EMI measurement can be theoretically described by equation (10) in terms of [27]:

$$\bar{Z}=\frac{1}{j\omega\cdot\bar{C}}\cdot\left\{1-\bar{k}_p^2\left[1-\frac{2}{\bar{\varphi}}\cdot\frac{J_1\left(\bar{\varphi}\right)}{J_0\left(\bar{\varphi}\right)}\cdot\frac{\bar{Z}_{P,\mathrm{sc}}}{\bar{Z}_{P,\mathrm{sc}}+\bar{Z}_{\mathrm{str}}}\right]\right\}^{-1} \tag{10}$$

where $\bar{C}=\frac{\bar{\varepsilon}_{33}^{T}\pi a^2}{h}$, $\bar{k}_p^2=\frac{2d_{31}^2}{\left[\bar{s}_{11}^{E}\cdot\bar{\varepsilon}_{33}^{T}(1-\nu)\right]}$, and $\bar{\varphi}=\frac{\omega\cdot a}{\bar{c}_p}$. The parameters in equation (10) have been presented in the nomenclatures table.

Due to the variation of the resin matrix properties, the DoC of the composite fluctuates in the curing process. Apart from $\bar{Z}_{\mathrm{str}}$, other parameters in equation (10) stay unchanged through the curing process since the ambient temperature is constantly kept at 120 °C. The $\bar{Z}_{\mathrm{str}}$ is only affected by the variation of structural properties through the curing process due to the chemical and physical reactions. Hence, the obtained EMI signals can be used for characterizing the curing progress in terms of equation (10).

FBG is a representative and widely used type of optical fiber grating, with a period typically in the sub-micron range. When light waves pass through the Bragg grating, a strong reflection is formed for light that satisfies the phase-matching condition. The phase-matching condition can be described in equation (11):

$$\lambda=2n_0\Lambda \tag{11}$$

where n_0 represents the effective refractive index of the grating region; Λ represents the grating period.

As can be seen from equation (11), FBG is sensitive to temperature and strain by inducing changes in n_0 and Λ, making them commonly used as temperature and strain sensors. The formulas for wavelength shift independently under the temperature and strain can be given by equations (12) and (13):

$$\Delta\lambda_T=\lambda\cdot\left(\frac{1}{\Lambda}\frac{\partial\Lambda}{\partial T}+\frac{1}{n_0}\frac{\partial n_0}{\partial T}\right)\cdot\Delta T \tag{12}$$

$$\Delta\lambda_\varepsilon=\lambda\cdot\left(\frac{1}{\Lambda}\frac{\partial\Lambda}{\partial\varepsilon}+\frac{1}{n_0}\frac{\partial n_0}{\partial\varepsilon}\right)\cdot\Delta\varepsilon \tag{13}$$

where $\Delta\lambda_T$ represents the wavelength shift induced by temperature, while $\Delta\lambda_\varepsilon$ denotes the wavelength shift induced by strain; ΔT and $\Delta\varepsilon$ are the variations of temperature and strain, respectively.

Table 1. Specifications of samples used in experiments.

	Specimens used in experiments	
Specifications	Source domain	Target domain
Plies number	10	8
Plies sequence	$[(0,90)]_{10}$	$[0]_8$
Overall size ($L \times W \times T$)	Composite patch: 100 mm × 100 mm × 2 mm. Aluminum plate: 300 mm × 300 mm × 3 mm	400 mm × 400 mm × 1.6 mm
Sensors	Diameter of piezoelectric wafers: 6 mm. Thickness: 0.5 mm	Optical fiber diameter: 8.2 μm. Optical fiber diameter with cladding: 125 μm

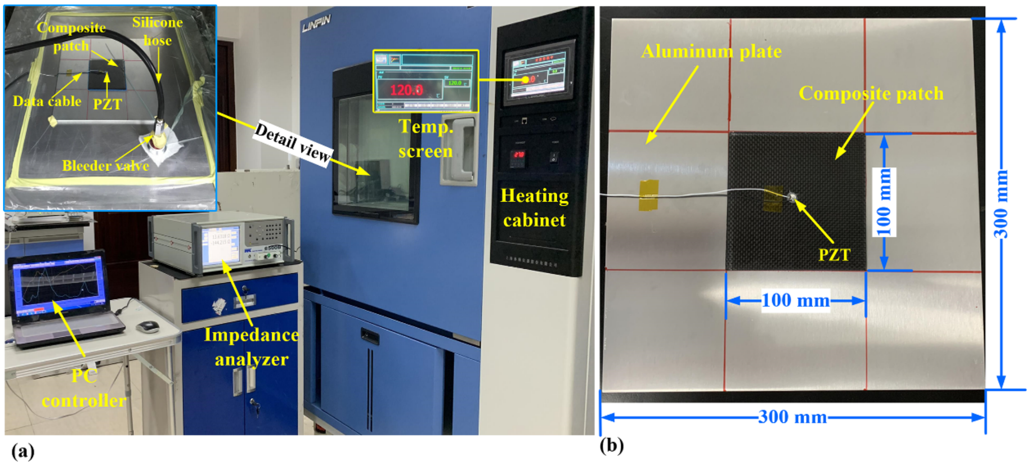

Figure 3. EMI measurement system for curing monitoring: (a) overall view, (b) co-cured specimen.

3. Experiments validation and datasets construction

3.1. Design of experiments

A series of experiments have been designed and carried out to validate the proposed approach in this study. As mentioned above, the experimental data are collected from EMI and FBG measurements based on the piezoelectric wafer and the optical fiber. The discrepancies leading to different curing regularity of composites consist in overall sizes, ply sequence, and materials, as shown in table 1.

Specifically, table 1 presents specifications for an experimental setup involving composite materials and sensor instrumentation. The source domain consists of ten plies with a complex $[(0,90)]_{10}$ stacking sequence, while the target domain employs eight plies with a simpler $[0]_8$ sequence. The composite patch measures 100 mm × 100 mm × 2 mm, accompanied by a 300 mm × 300 mm × 3 mm aluminum plate used in both domains. The target domain features a larger 400 mm × 400 mm × 1.6 mm composite patch. The source domain employs 6 mm diameter piezoelectric wafers (0.5 mm thick), while the target domain uses 8.2 μm diameter optical fibers, including a 125 μm cladding. These variations highlight material composition, size, and sensor types, which are crucial in this study.

3.1.1. EMI measurement configuration. The experiments in the source domain are designed to evaluate the curing process of composite structures using EMI. This specimen is a co-cured structure comprising composite and metal. The system of EMI measurement and fabricated samples are illustrated in figure 3.

Figure 3 shows that the testing platform comprises a WK6500B impedance analyzer (Wayne Kerr Electronics Ltd, London), a PC controller, and a heating facility. The impedance analyzer is connected to the piezoelectric transducer with heat-resistance wires. The analyzer obtains the data through the entire curing process. The PC controller is to manipulate the frequency from 100 kHz to 600 kHz with a step of 1 kHz. The heating time of the curing process is about 240 min, with a data sampling interval of 2 min, and 121 groups of raw data are obtained.

The specimen to be co-cured is made of aluminum plate 6061-T6 and T300 woven prepreg. The piezoelectric sensor is

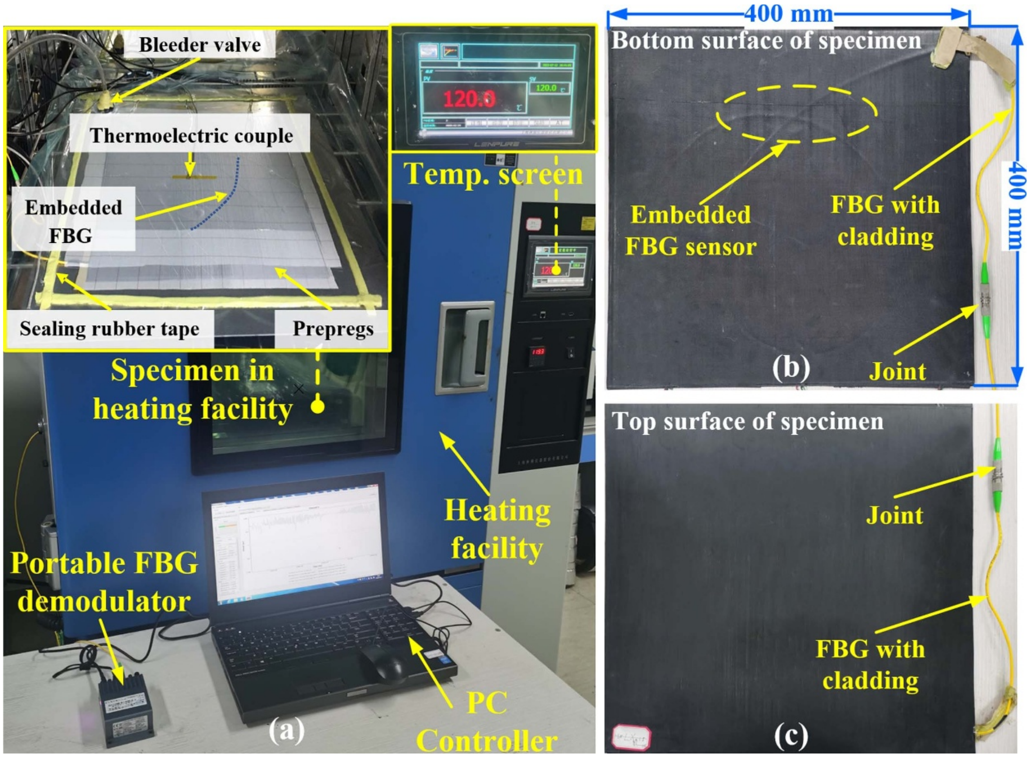

Figure 4. FBG measurement system for curing monitoring: (a) overall view, (b) bottom view of the specimen, (c) top view of the specimen.

actuated with a voltage magnitude of 1 V in the experiment. It should be noted that only the real part of EMI data is adopted for curing process evaluation due to its high sensitivity to structural variation.

3.1.2. FBG measurement configuration.

Another experiment is designed for the curing process measured by FBG sensors. The FBG data is the micro-strain, which varies with the curing process progressing. In this study, the DoC monitoring based on FBG data is a target task to test the extendibility of the proposed approach. The FBG measurement system is shown in figure 4(a). It contains a heating cabinet, a portable FBG demodulator (AeroGator, Technobis Fibre Technologies B.V.) with a maximum sampling frequency of 19.2 kHz in the length scope from 1515 nm to 1585 nm, and a controller. Figures 4(b) and (c) are separate bottom and top views of the cured specimen with an embedded optical fiber.

This experiment lasts 180 min with heating, alongside a data sampling interval of 3 min, and 63 groups of curing data are obtained at last. Considering the complexity of analyzing the initial FBG data, these are preprocessed with normalization before serving as a dataset in the target domain.

3.2. Dataset construction using raw sensor data

Although substantial efforts have been made in ML-related research for composites, insufficient data quantity still dramatically limits the development of competitive models. Thus, a simple but effective method, mean interpolation (MI), is applied to increase the quantity of the samples based on the originally obtained EMI and FBG data. MI is a simple method to estimate missing data points in a dataset. The operating principle involves calculating the average of neighboring data points on either side of the missing value. This average is then used to fill in the missing value, assuming that the missing point is likely to be close in value to its neighbors. MI method is quick and easy to operate but may not capture more complex patterns or variations in the data as effectively as more sophisticated interpolation methods.

3.2.1. Source domain dataset construction.

The number of initial samples measured by EMI is 121, but the sample quantity increases to 961 when enhanced with the MI. By trial and error, ten classes are determined with a DoC interval of 10%, which means $\text{DoC\_}i\in((i-1)\times 10\%,\ i\times 10\%)$ ($i = 1,2,3,\ldots,10$).

The EMI data, serving as the source domain dataset, is partitioned into training and testing sets with an 8:2 ratio. To improve the convergence performance and trainability of the CNN model, the data for training and testing are randomly shuffled. Herein, the task in the source domain is to implement a PBM model with high accuracy of DoC monitoring.

3.2.2. Target domain dataset construction.

The initial experimental data in the target domain are obtained via FBG measurement with the optical fiber, including six gratings. It is effortless to find out that there are discrepancies between the composite structures and collected raw data in the source and target domains.

Similarly, 497 samples are obtained in the enhanced dataset after being augmented with MI based on the initial FBG data in the target domain. Then, the FBG data in the enhanced dataset are also transformed into the GAF images. This image dataset is further split into training and testing sets to study the performance of the reconstructed model with the TL strategy. Based on the weight values of the PBM trained by the dataset in the source domain, the rebuilt CNN model driven by the TL strategy is adopted to quantify the DoC for the curing data from a new case comprising other composite structures, which is the target domain.

4. Results and discussion

4.1. Curing data collected by EMI and FBG measurements

The curve plots of the initial sensor data in the source and target domains are independently illustrated in figures 5(a) and (b). It should be noted that, in figure 5(a), the curves are manually selected with the step of 10 min to show the overall evolution regularity more intuitively.

As heating time increases, the peak frequency of the system shifts towards the right of the initial state curve (0 min), as shown in the plots in figure 5(a). In addition, the resistance magnitude decreases as the heating duration becomes longer. Figure 5(b) shows the normalized FBG data, which initially displays an increasing pattern before decreasing to zero. The peaks in figure 5(b) refer to the gel point, indicating the moment of phase transition. According to the results shown in figures 5(a) and (b), it demonstrates that EMI and FBG measurements can effectively characterize the curing process.

4.2. Transforming sensor data to GAF images

Transforming series data into images with GAF can capture relationships between data points. In the context of EMI and FBG signals mentioned in this study, the GAF conversion turns signal dynamics into structured images, aiding pattern recognition, feature extraction, and visualization. It is suitable for EMI and FBG signals because it can reveal complex patterns, invariant to time shifts, and simplify the communication of findings. Therefore, the GAF algorithm is suitable for converting the data of FBG and EMI into corresponding images.

To maximize the generalization capability of the TL method, the sensor data from experiments are herein converted into GAF images, which serve as the input of the proposed approach. However, owing to the great difficulties of showing all the transformed GAF images in one paper, only images at the initial and final stages through the curing process are presented, as shown in figures 6(a) and (b). It can be observed directly from these figures that the transformed GAF images present different features by comparison.

The transformed image using the EMI signature with 700 frequency points yields 700 pixels in horizontal and vertical directions, as shown in figure 6(a). Similarly, six pixels are distributed along the horizontal and vertical directions in figure 6(b), whose conversion is achieved based on the FBG signatures. It should be pointed out that the cross area in figure 6(a) is a counterpart to the peak frequency in figure 5(a). As the heating duration, the placement of the cross area gradually shifts from bottom-left to top-right.

4.3. DoC monitoring with TL strategy among different composites

As mentioned above, this study aims to implement the DoC monitoring between different composite structures by transferring the knowledge learned from the source domain to the target domain. Then, the training cost in the new scenario can be significantly lowered, accompanied by an improved ultimate performance.

4.3.1. Training a PBM on the EMI dataset of the source domain. This section describes training a basic CNN model to function as a PBM, with batch size set at 32 and epochs at 200 on the training set. The performance of the PBM is then verified on the testing set. The model training history curves using the source domain dataset are illustrated in figure 7.

Figure 7 displays four curves with double vertical axes. It is evident that two of the curves exhibit increasing and stable trends for accuracy, while the loss curves display decreasing and stable patterns. All four curves converge towards a constant value, indicating that the PBM exhibits superior convergent performance. Moreover, the minimal discrepancy between the training and testing curves signifies a well-trained CNN model.

Four broadly used metrics in the ML community, accuracy, precision, recall, and F1-score, are introduced herein to evaluate the PBM performance quantitatively. The evaluated PBM scores using the four indicators are enumerated in table 2. All indicator scores in the source domain are above 0.9500, confirming the superior performance of the PBM in accurately quantifying the DoC as defined in this study.

4.3.2. DoC monitoring on the FBG dataset of the target domain. As above mentioned, the TL strategy is employed on the target domain dataset. In this section, the PBM is utilized to extract features from the new dataset using the built-in frozen layers. The history curves on the target domain dataset changing with epochs are shown in figure 8.

Figure 8 shows that the two curves with a consistent upward trend represent accuracy plots, while the other two indicate

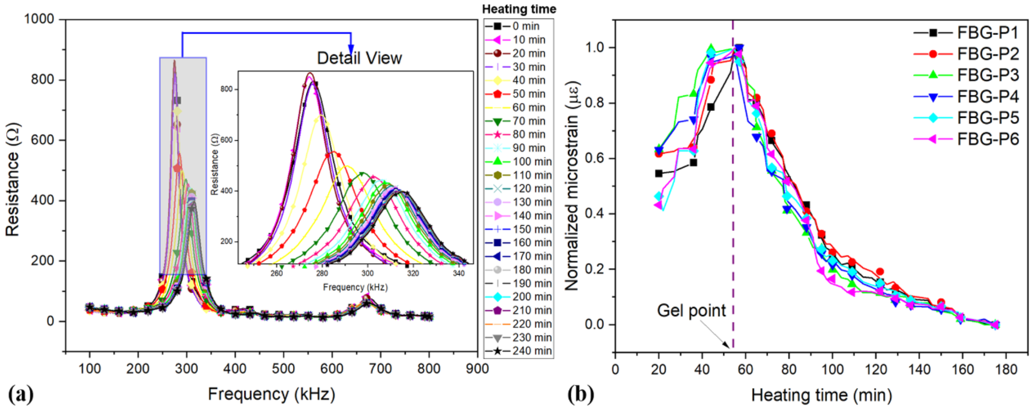

Figure 5. Plots of sensor data: (a) using EMI data, (b) using normalized FBG data.

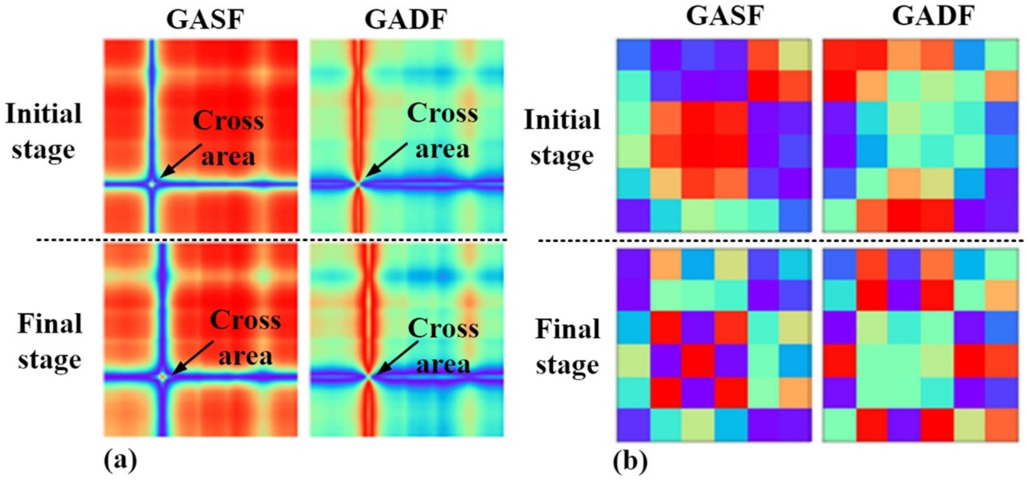

Figure 6. GAF at the initial and final stages: (a) using EMI dataset of the source domain, (b) using FBG dataset of the target domain.

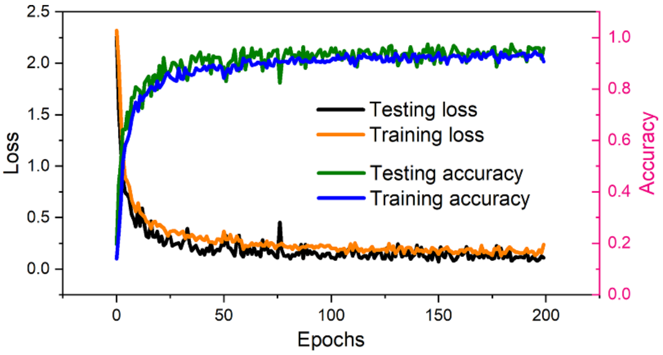

Figure 7. History curves of PBM using the EMI dataset of the source domain.

loss plots. The slight differences between the training and testing curves suggest that the reconstructed model can attain superior DoC quantitative identification outcomes within only 20 epochs.

Table 2. Indicator scores of the PBM on the dataset in source domain.

Indicators	Accuracy	Precision	Recall	F1
Scores	0.9585	0.9630	0.9587	0.9580

To investigate the performance of TL-boosted CNN on the testing dataset, a confusion matrix (CM) diagram is plotted, as shown in figure 9. Furthermore, to provide a more comprehensive and intuitive assessment of the model's performance, the CM is normalized to a scope of [0,1]. It should be noted that there are ten classes, ranging from DoC_1 to DoC_10, with the horizontal axis indicating the actual classes and the vertical axis representing the predicted classes. The numbers displayed in the grids of figure 9 indicate the percentage of correctly classified samples within each class. Based on the values presented in figure 9, it can be concluded that the DoC quantitative identification exhibits significantly high precision in every class.

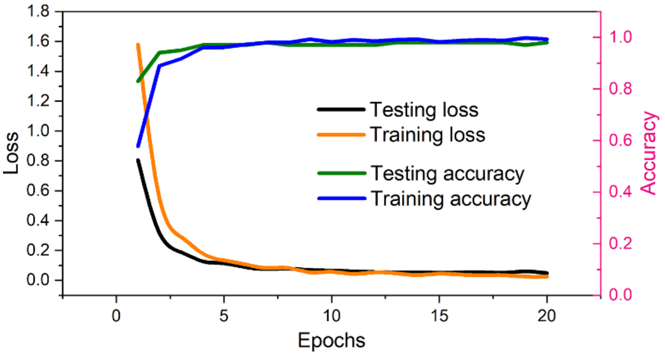

Figure 8. History plots of the rebuilt model on the FBG dataset of the target domain.

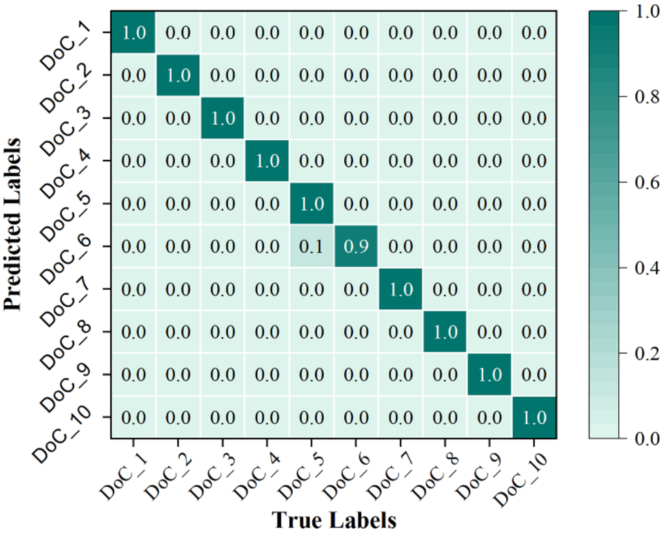

	DoC_1	DoC_2	DoC_3	DoC_4	DoC_5	DoC_6	DoC_7	DoC_8	DoC_9	DoC_10
DoC_1	1.0	0.0	0.0	0.0	0.0	0.0	0.0	0.0	0.0	0.0
DoC_2	0.0	1.0	0.0	0.0	0.0	0.0	0.0	0.0	0.0	0.0
DoC_3	0.0	0.0	1.0	0.0	0.0	0.0	0.0	0.0	0.0	0.0
DoC_4	0.0	0.0	0.0	1.0	0.0	0.0	0.0	0.0	0.0	0.0
DoC_5	0.0	0.0	0.0	0.0	1.0	0.0	0.0	0.0	0.0	0.0
DoC_6	0.0	0.0	0.0	0.0	0.1	0.9	0.0	0.0	0.0	0.0
DoC_7	0.0	0.0	0.0	0.0	0.0	0.0	1.0	0.0	0.0	0.0
DoC_8	0.0	0.0	0.0	0.0	0.0	0.0	0.0	1.0	0.0	0.0
DoC_9	0.0	0.0	0.0	0.0	0.0	0.0	0.0	0.0	1.0	0.0
DoC_10	0.0	0.0	0.0	0.0	0.0	0.0	0.0	0.0	0.0	1.0

Figure 9. Normalized CM of DoC quantitative identification with TL-boosted CNN on FBG dataset of the target domain.

Overall, the proposed TL-boosted CNN approach performs well on the target domain dataset for DoC quantitative identification. It only takes 6.58 s to be fully trained, compared to the 238.19 s required for PBM training on the same workstation. This reduction in training time consumption amounts to a remarkable 97.20% due to the avoidance of training a model from scratch using the FBG dataset of the target domain. Thus, the efficiency of the proposed approach in saving training time is clearly demonstrated.

4.3.3. Comparison between TL-boosted CNN and conventional ML algorithms. In this section, indicator scores of the developed TL-boosted CNN approach are compared with those of the conventional ML methods, such as DT, *k*-nearest neighbors (KNN), support vector machine (SVM), and Gaussian naïve Bayes (GNB). The proposed approach and the above ML algorithms are all evaluated on the same FBG dataset of the target domain to determine their performance.

To visually compare the performance of TL-boosted CNN and the usual ML methods, a bar graph is created and illustrated in figure 10. The graph is color-coded, and the bar height represents the magnitude of the score, with greater height indicating better performance. A table displaying all indicators is attached to the bar graph to provide exact numeric values. According to figure 10, the rebuilt model driven by the TL approach significantly outperforms the classic ML methods of DT, KNN, SVM, and GNB. The scores of the TL-boosted CNN model are specifically highlighted in orange to emphasize their superiority over conventional methods.

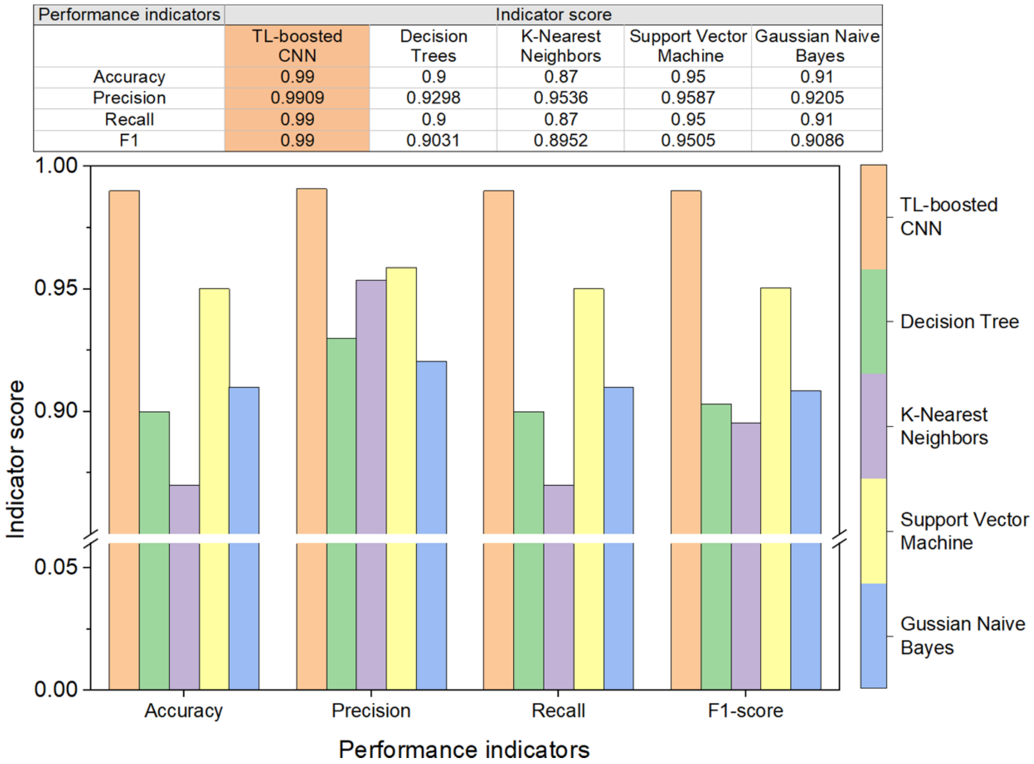

Performance indicators	Indicator score				
	TL-boosted CNN	Decision Trees	K-Nearest Neighbors	Support Vector Machine	Gaussian Naive Bayes
Accuracy	0.99	0.9	0.87	0.95	0.91
Precision	0.9909	0.9298	0.9536	0.9587	0.9205
Recall	0.99	0.9	0.87	0.95	0.91
F1	0.99	0.9031	0.8952	0.9505	0.9086

Figure 10. Comparison of the proposed approach and four conventional ML methods on the FBG dataset in the target domain.

5. Conclusions

This study presents a new way to monitor the curing process of polymeric composites at the cradle stage, which has important implications for improving their quality and service performance. Our main objective is to develop an effective approach for monitoring the curing process and quantifying the DoC of polymeric composite materials with the utilization of relevant data from other similar cases. Thus, we present an approach comprising GAF transformation, CNN model, and TL strategy, to improve the accuracy and efficiency of curing monitoring of composite structures.

The proposed approach is evaluated with the performance indicators, achieving scores above 0.9900 in quantifying the DoC on the FBG data of the target domain, with a reduction of training time up to 97.20% alongside enhancing the model generalization capacity. The proposed approach also indicates a significant improvement in the accuracy of DoC monitoring over conventional ML algorithms regarding indicator scores for performance evaluation.

Despite the inspiring results, there are still limitations to this study, such as the necessity for further validation on larger datasets and more extensive types of composites. In the follow-up research, we plan to modify this approach using multiple source domains with more complicated features and explore its potential applications in other industrial fields using various composite structures, such as aerospace, wind energy, transportation, etc.

Data availability statement

All data that support the findings of this study are included within the article (and any supplementary files).

Acknowledgments

Dr Jianjian Zhu acknowledges the project supported by the Young Scientists Fund of the National Natural Science Foundation of China (Grant No. 52205171). Professor Zhongqing Su acknowledges the support from the Hong Kong Research Grants Council via General Research Funds (Grant Nos. 15202820 and 15204419).

References

[1] Zhu J J, Wen J S, Chen C Y, Liu X, Lan Z F, Wang Y S and Qing X L 2022 Curing monitoring of bonded composite patch at constant temperature with electromechanical impedance and system parameters evaluation approach *Smart Mater. Struct.* **31** 015039

[2] Tang Z S, Lim Y Y, Smith S T and Padilla R V 2020 Modelling of the electromechanical impedance technique for prediction of elastic modulus of structural adhesives *Struct. Health Monit.* **20** 2245–60

[3] Liu X, Li Y K, Zhu J J, Wang Y S and Qing X L 2021 Monitoring of resin flow front and degree of cure in vacuum-assisted resin infusion process using multifunctional piezoelectric sensor network *Polym. Compos.* **42** 113–25

[4] Lim Y Y, Tang Z S and Smith S T 2019 Piezoelectric-based monitoring of the curing of structural adhesives: a novel experimental study *Smart Mater. Struct.* **28** 015016

[5] Tenreiro A F G, Lopes A M and da Silva L F 2022 A review of structural health monitoring of bonded structures using electromechanical impedance spectroscopy *Struct. Health Monit.* **21** 228–49

[6] Fan X Y, Li J and Hao H 2021 Review of piezoelectric impedance based structural health monitoring: physics-based and data-driven methods *Adv. Struct. Eng.* **24** 3609–26

[7] Aabid A, Parveez B, Raheman M A, Ibrahim Y E, Anjum A, Hrairi M, Parveen N and Zayan J M 2021 A review of piezoelectric material-based structural control and health monitoring techniques for engineering structures: challenges and opportunities *Actuators* **10** 101

[8] Jiao P C, Egbe K J I, Xie Y W, Nazar A M and Alavi A H 2020 Piezoelectric sensing techniques in structural health monitoring: a state-of-the-art review *Sensors* **20** 3730

[9] Priyadharshini M, Balaji D, Bhuvaneswari V, Rajeshkumar L, Sanjay M R and Siengchin S 2022 Fiber reinforced composite manufacturing with the aid of artificial intelligence—a state-of-the-art review *Arch. Comput. Method* E **29** 5511–24

[10] Lin Y and Guan Z D 2021 The use of machine learning for the prediction of the uniformity of the degree of cure of a composite in an autoclave *Aerospace* **8** 130

[11] Lavaggi T, Samizadeh M, Kermani N N, Khalili M M and Advani S G 2022 Theory-guided machine learning for optimal autoclave co-curing of sandwich composite structures *Polym. Compos.* **43** 5319–31

[12] Hou J T, You B, Xu J Z and Wang T 2022 Prediction of curing process for thermosetting prepreg compression molding process based on machine learning *Polym. Compos.* **43** 1749–62

[13] Hassani S, Mousavi M and Gandomi A H 2022 Structural health monitoring in composite structures: a comprehensive review *Sensors* **22** 153

[14] Thai H T 2022 Machine learning for structural engineering: a state-of-the-art review *Structures* **38** 448–91

[15] Bao Y Q and Li H 2021 Machine learning paradigm for structural health monitoring *Struct. Health Monit.* **20** 1353–72

[16] Qing X L, Liao Y L, Wang Y H, Chen B Q, Zhang F H and Wang Y S 2022 Machine learning based quantitative damage monitoring of composite structure *Int. J. Smart Nano Mater.* **13** 167–202

[17] Szabelski J, Karpinski R and Machrowska A 2022 Application of an artificial neural network in the modelling of heat curing effects on the strength of adhesive joints at elevated temperature with imprecise adhesive mix ratios *Materials* **15** 721

[18] Jin K, Luo H, Wang Z Y, Wang H and Tao J 2020 Composition optimization of a high-performance epoxy resin based on molecular dynamics and machine learning *Mater. Design* **194** 108932

[19] Pruksawan S, Lambard G, Samitsu S, Sodeyama K and Naito M 2019 Prediction and optimization of epoxy adhesive strength from a small dataset through active learning *Sci. Technol. Adv. Mater.* **20** 1010–21

[20] Doblies A, Boll B and Fiedler B 2019 Prediction of thermal exposure and mechanical behavior of epoxy resin using artificial neural networks and Fourier transform infrared spectroscopy *Polymers* **11** 363

[21] Pan S J and Yang Q 2009 A survey on transfer learning *IEEE Trans. Knowl. Data Eng.* **22** 1345–59

[22] Zhuang F, Qi Z, Duan K, Xi D, Zhu Y, Zhu H, Xiong H and He Q 2020 A comprehensive survey on transfer learning *Proc. IEEE* **109** 43–76

[23] Rawat W and Wang Z 2017 Deep convolutional neural networks for image classification: a comprehensive review *Neural Comput.* **29** 2352–449

[24] Dhruv P and Naskar S 2020 Image classification using convolutional neural network (CNN) and recurrent neural network (RNN): a review *Machine Learning and Information Processing* (Springer) pp 367–81

[25] Li S, Song W, Fang L, Chen Y, Ghamisi P and Benediktsson J A 2019 Deep learning for hyperspectral image classification: an overview *IEEE Trans. Geosci. Remote Sens.* **57** 6690–709

[26] Wang Z and Oates T 2015 Imaging time-series to improve classification and imputation *24th Int. Joint Conf. on Artificial Intelligence*

[27] Zhu J J, Wang Y S and Qing X L 2019 A novel electromechanical impedance model for surface-bonded circular piezoelectric transducer *Smart Mater. Struct.* **28** 105052